Available online at www.sciencedirect.com

ScienceDirect

Geochimica et Cosmochimica Acta 140 (2014) 80–94

Geochimica et Cosmochimica Acta

www.elsevier.com/locate/gca

Oxygenation of Ediacaran Ocean recorded by iron isotopes

Haifeng Fan [a,b], Xiangkun Zhu [a,*], Hanjie Wen [b], Bin Yan [a], Jin Li [a], Lianjun Feng [c]

[a] *Laboratory of Isotope Geology, State Key Laboratory of Continental Tectonics and Dynamics, Institute of Geology, Chinese Academy of Geological Sciences, Beijing 100037, China*

[b] *State Key Laboratory of Ore Deposit Geochemistry, Institute of Geochemistry, Chinese Academy of Sciences, Guiyang 550002, China*

[c] *Institute of Geology and Geophysics, Chinese Academy of Sciences, Beijing 100029, China*

Received 17 December 2013; accepted in revised form 19 May 2014; available online 2 June 2014

Abstract

The increase in atmospheric oxygen during the late Neoproterozoic Era (ca. 800–542 Ma) may have stimulated the oxygenation of the deep oceans and the evolution of macroscopic multicellular organisms. However, the mechanism and magnitude of Neoproterozoic oxygenation remain uncertain. We present Fe isotopes, Fe species and other geochemical data for two sections of the Doushantuo Formation (ca. 635–551 Ma) deposited after the Nantuo glacial episode in the Yangtze Gorge area, South China. It is highlighted that highly positive $\delta^{56}Fe$ values reflect a lower oxidation rate of $Fe(II)_{aq}$ under ferruginous conditions, and in turn near zero $\delta^{56}Fe$ values indicate oxidizing conditions. Our study suggests that during the deposition of the bottom of Member II of the Doushantuo Formation the shallow seawater was oxic, but the deep water was characterized by ferruginous conditions, which is consistent with a redox chemical stratification model. Subsequent anoxic conditions under shallow seawater, represented by positive $\delta^{56}Fe$ and negative $\delta^{13}C_{carb}$ excursions, should be ascribed to the upwelling of $Fe(II)_{aq}$ and dissolved organic carbon (DOC)-rich anoxic deep seawater. The oxidation of Fe $(II)_{aq}$ and DOC-rich anoxic deep seawater upon mixing with oxic shallow water provides an innovative explanation for the well-known negative $\delta^{13}C_{carb}$ excursions (ENC2) and positive $\delta^{56}Fe$ excursions in the middle of Doushantuo Formation. Meanwhile, the upwelling Fe $(II)_{aq}$- and DOC-rich anoxic deep seawater could increase photosynthetic activity. The balance between oxygen consumption and production was most important criteria for the oxygenation of Early Ediacaran Ocean and diversity of eukaryotic organisms.

1. INTRODUCTION

A significant change of Earth surface redox is thought to have occurred during the late Neoproterozoic, and is often referred to as the "Neoproterozoic Oxygenation Event" (Canfield, 2005; Shields-Zhou and Och, 2011). However, the mechanism and magnitude of the oxygenation event have not been well constrained. Several lines of geochemical evidence suggest that the Ediacaran (635–541 Ma) surface and deep ocean became oxygenated. The evidence includes the increase of sulfur isotopic fractionation between coexisting sulfide and sulfate (Fike et al., 2006), the lower ratio between highly reactive Fe (Fe_{HR}) and total Fe (Fe_T) (Canfield et al., 2007), the enrichment of redox-sensitive trace elements (Sahoo et al., 2012) and the significant negative $\delta^{13}C_{carb}$ excursion (Fike et al., 2006; McFadden et al., 2008). Recently, the oxygenation model for the Ediacaran Ocean has been challenged by a redox chemical stratification model, with oxic surface water underlain by a thin ferruginous layer, an euxinic wedge and ferruginous deep water (Li et al., 2010).

Many studies have focused on Ediacaran chemo-stratigraphic correlation by coupling carbon, oxygen and sulfur isotopes, in which striking negative $\delta^{13}C_{carb}$ excursions were

* Corresponding author. Tel./fax: +86 1068999798.
E-mail address: xkzhu0824@gmail.com (X. Zhu).

http://dx.doi.org/10.1016/j.gca.2014.05.029
0016-7037/

recorded. The remarkable negative $\delta^{13}C_{carb}$ excursions have been observed not only in the Doushantuo Formation of South China (McFadden et al., 2008; Jiang et al., 2011; Zhu et al., 2013), but also in equivalent strata from other sites worldwide (Fike et al., 2006; Bjerrum and Canfield, 2011). Most authors have suggested that the negative $\delta^{13}C_{carb}$ excursions reflect seawater column stratification and the oxygenation of a large DOC reservoir sourced from anoxic deep seawater (Fike et al., 2006; Jiang et al., 2007; McFadden et al., 2008). This popular interpretation has also been challenged by alternative scenarios involving secondary alteration by meteoric water and burial diagenesis (Knauth and Kennedy, 2009; Derry, 2010).

The Fe isotopic composition of modern and ancient marine sedimentary rocks and minerals, such as banded iron formations, pyrites in black shale, and carbonates, is useful for understanding the redox condition of seawater and Fe geochemical cycling (Johnson et al., 2003, 2008; Rouxel et al., 2005; Yamaguchi et al., 2005; Zhu et al., 2008a; Duan et al., 2010; Asael et al., 2013). The dissolved $Fe(II)_{aq}$ in surface water is commonly oxidized by abiotic and biotic processes to form ferric oxides, which result in the enrichment of the heavier Fe isotopes in ferric oxide (hematite, goethite and magnetite) with fractionation relative to $Fe(II)_{aq}$ ranging from 1‰ to 3.5‰ (Bullen et al., 2001; Johnson et al., 2002; Welch et al., 2003; Croal et al., 2004). Under anoxic and euxinic conditions, $Fe(II)_{aq}$ would preferentially be precipitated as an FeS_m phase or pyrite into sediments. This would promote the accumulation of the lighter Fe isotopes in the sediments as the authigenic FeS_m phase and pyrite have isotope fractionations ranging from −0.3‰ to −3.0‰ (Rouxel et al., 2005; Butler et al., 2005; Guilbaud et al., 2011; Zhu et al., 2008a; Wu et al., 2012a). However, highly negative $\delta^{56}Fe$ values in Precambrian ferric oxides were also reported, which is commonly interpreted as the presence of microbial Fe(III)-reduction (Beard et al., 2003; Yamaguchi et al., 2005; Johnson and Beard, 2005). Highly positive $\delta^{56}Fe$ values in Precambrian pyrites reflect the diagenetic origin of these pyrites after ferric oxides (Nishizawa et al., 2010; Fabre et al., 2011; Yoshiya et al., 2012). Ferrous carbonates (e.g., siderite, ankerite) can also be part of the iron sink in ancient oceanic systems. These ferrous carbonates usually show negative $\delta^{56}Fe$ values at isotopic equilibrium conditions (Yamaguchi et al., 2005; Frost et al., 2007; Von Blanckenburg et al., 2008), consistent with experimental studies that estimate isotope fractionation ranging from −0.5‰ to −0.9‰ between ferrous carbonate and $Fe(II)_{aq}$ (Wiesli et al., 2004; Johnson et al., 2005).

Here we present Fe and carbon isotopes, and other geochemical data of cherts, carbonates and phosphorites from Early Ediacaran Doushantuo Formation (Member II–III) in South China, to trace the redox environment of Ediacaran Ocean and to constrain the oxidation mechanism of DOC. Together with their deposition condition, our data highlight that Ediacaran seawater can be characterized by a redox chemical stratification model and that the oxidation of upwelling $Fe(II)_{aq}$- and DOC-rich anoxic deep water into oxic shallow water could be an important mechanism controlling these redox conditions.

2. GEOLOGICAL SETTING AND STRATIGRAPHY

Ediacaran successions in South China developed on a south-southeast facing (present day position) passive margin on the Yangtze Craton after the breakup of Rodinia about 850–750 Ma (Wang and Li, 2003). The Cryogenian glacial and interglacial successions (750–635 Ma) record rift-drift transition, although there is a lack of the exact timing of the rifting events in China (Jiang et al., 2003). Subsequent Ediacaran deposition (635–541 Ma) occurred in a marginal environment and focused on topographic highs and lows created by fault blocks during development of the Nanhua Rift system (Jiang et al., 2003; Zhu et al., 2007).

The Ediacaran successions, including Doushantuo and Dengying (or Liuchapo) Formations in South China, display a significant variation of strata thickness from >1000 m in the shallow water platform to <250 m in the deep marine basin (Zhu et al., 2007, 2013; Jiang et al., 2007, 2011). The Doushantuo Formation is underlain by the Cryogenian Nantuo Formation diamictite and overlain by Dengying Formation peritidal dolostone and organism-rich limestone (e.g., Jiang et al., 2007, 2011; McFadden et al., 2008, 2009; Zhu et al., 2007, 2013). The age of Doushantuo Formation in the Yangtze Gorges area has been constrained between 635.2 ± 0.6 Ma and 551.1 ± 0.7 Ma by zircon U–Pb ages obtained from interbedded volcanic ash (Condon et al., 2005). The Doushantuo Formation which varies in thickness from 90 to 200 m, was deposited under subtidal or intertidal conditions and is usually divided into four different lithologic members (McFadden et al., 2008; Jiang et al., 2011) (Fig. 1). Member I is a 5 m-thick cap dolostone. Member II (80–120 m thick) contains alternating black shale and dolostone with abundant pea-sized fossiliferous cherty nodules. Member III consists of 40–60 m massive and laminated dolostones interbedded with cherty bands or lenses. In both Member II and III, these cherty nodules and bands preserved abundant silicified microfossils including acritarchs, coccoidal and filamentous cyanobacterial, multicellular algae, doubtful embryos and tubular microfossils (e.g., Xiao, 2004; McFadden et al., 2009; Liu et al., 2013). Recent biostratigraphic studies suggested that the lower biozone (*Tianzhushania spinosa* and *Meghystrichosphaeridium magnificum*) and the upper biozone (*Ericiasphaera rigida* and *Tianzhushania spinosa*) persevered in early diagenetic cherty nodules and bands can be easily identified in most of sections of the Doushantuo Formation (McFadden et al., 2009; Liu et al., 2013). Member IV is a layer of 10 m thick black organism-rich shale, siliceous shale, or mudstone.

In this study, the Baiguoyuan (BGY) section (shallower water) and the Liuhuiwan (LHW) section (deeper water) were investigated. Their locations and stratigraphies were well described by Zhu et al. (2013) and Liu et al. (2013) (Fig. 1). The Baiguoyuan section is located at N31°19′31.1″, E111°03′33.1″ in the northwestern limb of the Huangling Anticline (Fig. 1A). Aside from the lowermost part (Member I), the Doushantuo Formation is well exposed. The lowest exposed part of the Doushantuo

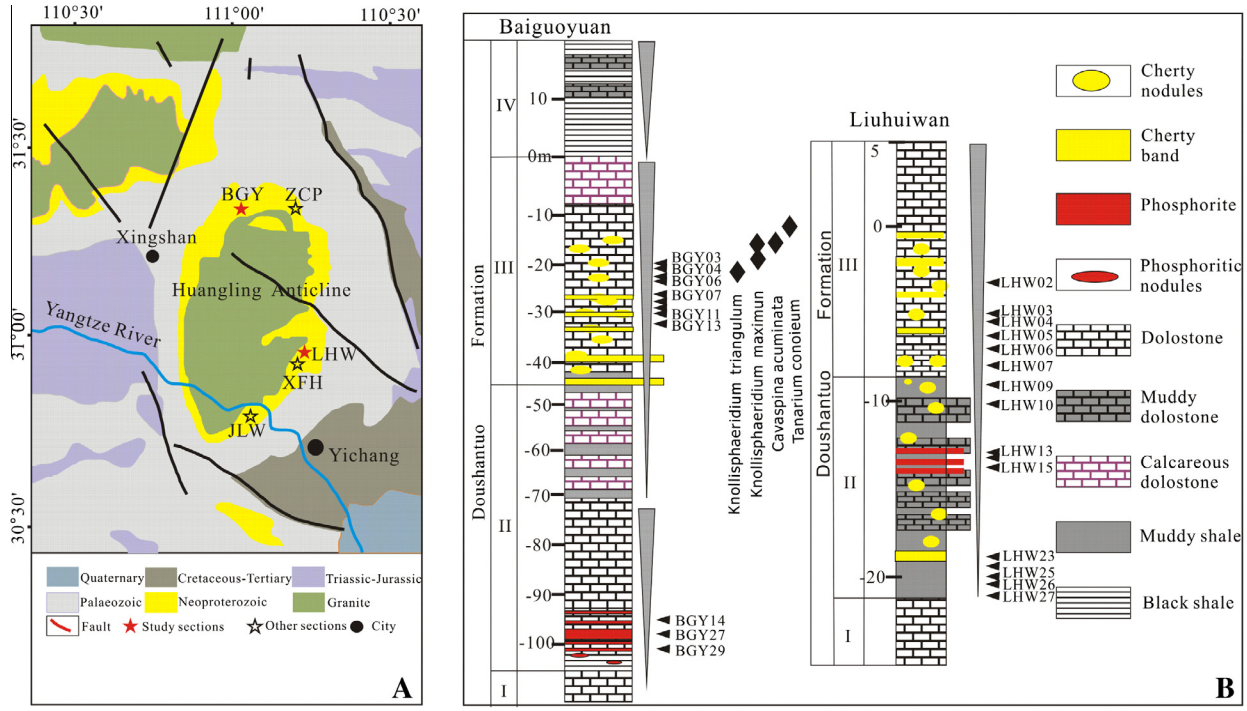

Fig. 1. Geological map of Yangtze Gorge area (A), locations and stratigraphic correlation of the Liuhuiwan section and the Baiguoyuan section (B), modified from Zhu et al. (2013) and Liu et al. (2013). Sample locations also have been shown in Fig. 1B.

Formation in this section contains ~4 m of dark phosphorites interbedded with dolostones (Fig. 1B). The phosphorite unit is succeeded by a 4 m-thick unit of grey, thick-bedded dolostone, followed by 20 m-thick dolostone and 30 m-thick black silty shale with muddy dolostone interlayer (Member II). This unit was followed by an ~50 m grey middle-thick dolostone (Member III), in which abundant cherty nodules or irregular cherty bands are occasionally observed (Fig. 1B). In these cherty nodules of Member III, four acritarch species have been identified, including *Cavaspina acuminata, Knollisphaeridium maximum, Knollisphaeridium triangulum* and *Tanarium conoideum* (Liu et al., 2013, Fig. 1B). At the top of the section, a 15 m-thick black shale hosts thin dolostone layers and represents Member IV.

The Liuhuiwan section is located near the village of Liuhuiwan, ~2 km north of Xiaofeng town (N30°57′11.3″, E111°16′59.2″, Fig. 1A). Recent field investigation indicated that Member IV is absent on the east limb (from Liuhuiwan to Niuping) of the Huangling Anticline (Liu et al., 2013, Fig. 1B). The section represents the best exposure of an important transitional succession (shale-dominated facies to carbonate-dominated facies) in the middle of the second sequence of the Doushantuo Formation in the southern Huangling Anticline. This succession is generally not well exposed in other sections from the Yangtze Gorges area. The basal 10 m succession is composed of intercalated dark grey laminated dolostone and shale with abundant cherty nodules (Fig. 1B). Up the section, there is a 2.5 m thick unit of massive dolostone with abundant cherty nodules overlain by 1.5 m of phosphorite interbedded with muddy dolostone, cherty bands and nodules (Fig. 1B). Further up the section, there is a cliff section composed of ~6.5 m of thick grey dolostone which contains abundant irregular cherty bands and nodules. At the top of the section, there is a layer of whitish grey dolomitic grainstone without cherty nodules and bands.

3. SAMPLES AND METHODS

3.1. Sample description

The freshest large block samples, including cherts (cherty nodules and bands), dolostones and phosphorites, were collected from the Doushantuo Formation (Members II and III) at the Baiguoyuan and Liuhuiwan sections in the Yangtze Gorge area (Fig. 1B). The diameters of the cherty nodules that occurred in the dolostone and mudstone range from several millimeters to a couple of centimeters (Fig. 2A). These cherty nodules usually contain high organic carbon and disseminated pyrite (Xiao et al., 2010), and control the distribution of acanthomorphic acritarchs (McFadden et al., 2009; Liu et al., 2013). The cherty bands occur as 1–10 cm thick discrete bands interbedded with dolostones and mudstones in the field (Fig. 2B). These cherty bands contain rare acanthomorphic acritarchs but also other abundant microfossils (McFadden et al., 2009). These cherts (nodules and bands) are composed of about 80–96% or more silica, present as microcrystalline, micro- and mega-quartz, and a few carbonate minerals (Fig. 2C and D) which suggest that these cherts formed by replacement of primarily carbonate with silica-rich solution during early diagenesis (Xiao et al., 2010). There are also a few quartz veins crossing through the early diagenetic quartz and carbonates (Fig. 2C). We propose

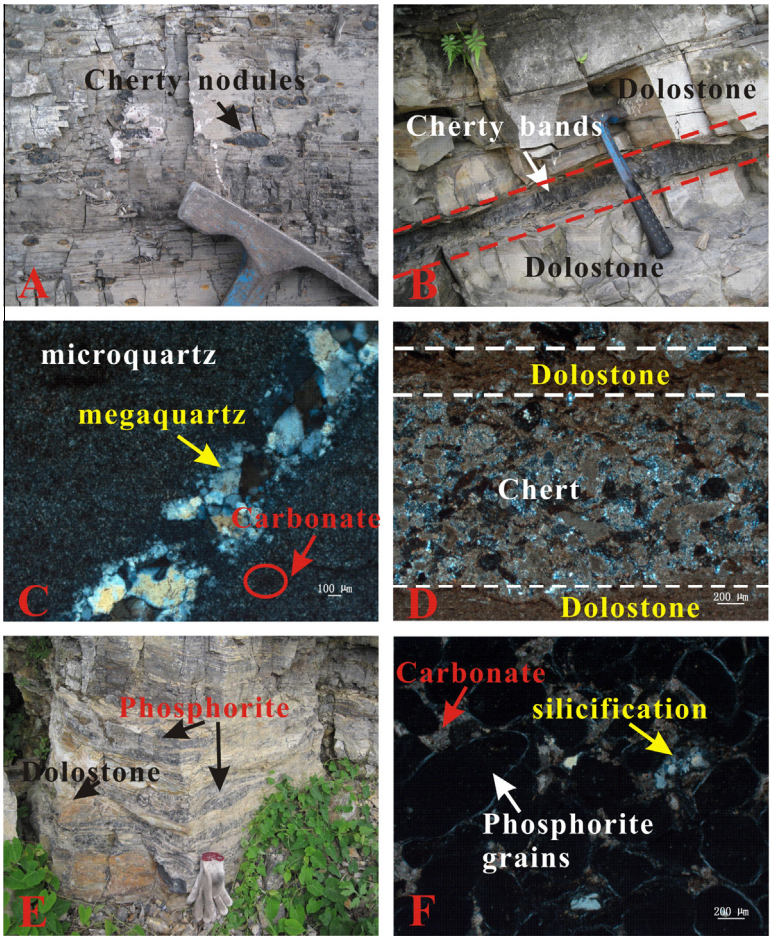

Fig. 2. (A and B) Field photographs of cherts (nodules and bands) from Doushantuo Formation in the Yangtze Gorge area. (C and D) Thin section photomicrographs of two chert samples (LHW25 and BGY07) indicated that cherts would be formed likely by the means of replacement of carbonate sediments with silica-rich solution which has taken place before compaction and calcite cementation (Xiao et al., 2010). However, direct precipitation of dissolved silica from the ambient seawater cannot be excluded. (E) Field photography of phosphorite at lower part of the Baiguoyuan section; (F) Thin section of a phosphorite (BGY14), phosphatic grains in total extinction under cross-polarized transmitted light.

that these cherty bands could also include some products formed by direct precipitation of dissolved silica from ambient seawater, based on the texture of the microquartz and carbonate (Fig. 2C and D). Phosphorite bands (2–10 cm) in the two sections are interbedded with dolostones (Fig. 2E). Silicification also can be observed in these phosphorites (Fig. 2F).

3.2. Analytical methods

3.2.1. Major and trace element analyses

The potential weathered surfaces of samples have been removed by cutting machine before crushing into powders for chemical analysis. The major elements of twenty-eight samples were measured by X-ray fluorescence (XRF) using lithium tetraborate powder pelleting at the ALS Chemex (Guangzhou) Co., Ltd. The standard reference materials (SRM) were analyzed together with unknown samples and the results suggested that the accuracy is better than 5%.

The trace element concentrations were analyzed using an ICP-MS at the Institute of Geochemistry, Chinese Academy of Sciences. All samples were first ashed at 500 °C to remove organic materials. Subsequently, the ashed samples were digested with a mixture of HNO_3 and HF acids at 130 °C for 72 h in a clean room. A small aliquot of digestion solution was taken for trace element concentration. The accuracy is better than 3%, which is calculated from the results of standard reference materials such as GBPG-1 (Garnet-Biotite Plagiogneiss), OU-6 (Penrhyn Slate) and AMH-1 (Mount Hood Andesite) (Qi et al., 2000).

3.2.2. Fe isotope analysis

The chemical purification of dissolved whole rocks for Fe isotope analysis was carried out by AGMP-1 resin following the method from Zhu et al. (2008b) and Zhao et al. (2012). Fe isotopic compositions were measured using a Nu–MC–ICP–MS at the Institute of Geology, Chinese Academy of Geological Sciences. Fe isotopic results are expressed in the standard notation as δ^{56}Fe deviation from IRMM-014. Accuracy of each analytical run and long-term reproducibility were tested by routine analyses of two lab standards (CAGS-Fe, GSR-3) and an international

Table 1
Chemical composition, iron and carbon isotopic composition of samples in the Baiguoyuan (BGY) section and the Liuhuiwan (LHW) section.

Sample	Description	Depth(m)	$\delta^{57}Fe_{WR}$		$\delta^{56}Fe_{WR}$		$\delta^{13}C_{Car}$	SiO_2 (%)	Al_2O_3 (%)	Fe_2O_3 (%)	P_2O_5 (%)	TREE (ppm)	Zr (ppm)	Fe/Al
			‰	2σ	‰	2σ								
The Liuhuiwan section														
LHW02	Chert	−3.5	1.41	0.19	0.94	0.07	2.34	92.21	0.17	0.07	0.64	19.21	1.87	0.54
LHW03	Chert	−5.0	1.88	0.15	1.26	0.08	0.28	75.11	0.19	0.05	0.17	6.46	2.29	0.35
LHW03	Duplicated	−5.0	1.89	0.16	1.26	0.10								0.35
LHW04	Chert	−6.0	1.84	0.20	1.13	0.17	−0.47	93.85	0.15	0.06	0.42	12.65	2.90	0.53
LHW05	Chert	−6.5	1.38	0.10	0.94	0.17	−0.19	86.85	0.26	0.08	0.22	8.38	3.80	0.41
LHW06	Dolostone	−7.0	0.69	0.09	0.47	0.11	−0.67	9.03	0.81	0.41	0.95	28.40	6.85	0.67
LHW07	Chert	−8.0	1.14	0.08	0.76	0.08	−2.03	84.03	0.17	0.10	0.48	9.08	2.19	0.78
LHW09	Chert	−9.0	0.98	0.15	0.65	0.13	−0.70	77.26	0.22	0.12	1.60	16.38	3.01	0.72
LHW10	Chert	−10.5	0.42	0.06	0.23	0.06	−1.10	86.31	0.18	0.07	0.58	16.28	3.10	0.51
LHW13	Chert	−12.8					−0.19	87.92	0.07	0.01	0.10	1.26	0.59	0.19
LHW14	Chert	−13.0					−0.40	92.75	0.08	0.01	0.06	0.86	0.54	0.17
LHW15	Phosphorite	−13.9	0.62	0.12	0.44	0.06	0.80	5.65	0.50	0.24	17.85	145.24	9.70	0.63
LHW23	Chert	−18.0	0.37	0.08	0.25	0.04	1.74	67.98	0.33	0.45	0.11	13.52	3.76	1.80
LHW23	Duplicated	−18.0	0.32	0.17	0.20	0.04								
LHW24	Chert	−19.0	0.92	0.01	0.66	0.05	1.47	77.51	0.33	0.14	0.58	20.20	3.32	0.56
LHW25	Chert	−20.0	0.73	0.19	0.42	0.23	2.87	80.56	0.19	0.18	0.40	14.17	4.27	1.25
LHW26	Chert	−21.0	0.63	0.13	0.42	0.09		84.51	0.15	0.03	0.68	15.52	2.14	0.26
LHW27	Dolostone	−22.0	0.65	0.01	0.43	0.05	2.08	11.81	1.06	0.71	0.68	29.65	16.80	0.89
The Baiguoyuan section														
BGY03	Chert	−20	−‘				1.26	95.85	0.12	0.05	0.51	16.74	2.50	0.55
BGY04	Chert	−20.5	0.40	0.20	0.29	0.21	2.34	86.71	0.53	0.26	0.70	71.67	19.80	0.65
BGY05	Chert	−22.5	0.31	0.19	0.22	0.20	−3.39	95.50	0.31	0.10	0.53	51.57	8.23	0.43
BGY06	Dolostone	−23	0.61	0.13	0.39	0.09	0.18	10.89	0.58	0.29	0.26	28.50	8.73	0.66
BGY07	Chert	−27.5	–				−0.34	92.85	0.07	0.02	0.04	3.25	0.92	0.36
BGY08	Chert	−28.7	0.94	0.03	0.61	0.04	1.51	93.50	0.25	0.78	0.18	10.18	2.63	4.13
BGY08	Duplicated	−28.7	0.95	0.02	0.63	0.15								
BGY10	Chert	−29	1.30	0.01	0.89	0.04	4.29	94.76	0.15	0.14	0.07	6.79	2.55	1.23
BGY11	Dolostone	−30	0.25	0.16	0.18	0.10	5.70	14.14	0.88	0.59	0.07	23.13	10.50	0.89
BGY13	Chert	−33	0.73	0.22	0.54	0.20	5.54	82.00	0.13	0.05	0.03	6.80	1.71	0.51
BGY14	Phosphorite	−94	0.79	0.05	0.54	0.02	−5.77	17.77	0.22	0.45	32.12	537.55	14.60	2.70
BGY14	Duplicated	−94	0.74	0.08	0.50	0.06								
BGY27	Phosphorite	−96	0.06	0.08	0.07	0.03	−4.76	14.96	3.78	0.83	30.31	204.59	48.10	0.29
BGY29	Phosphorite	−100	0.12	0.13	0.09	0.01	−2.51	11.55	2.20	0.91	31.54	198.64	32.90	0.55
The results of Geostandards														
BCR-2		Basalt		0.116			0.08		0.07		0.06		Our lab, Zhao et al. (2012)	
				0.116			0.08		0.09		0.01		Craddock and Dauphas (2011)	
GSR-3		Basalt		0.23			0.08		0.14		0.09		This study	
				0.232			0.028		0.154		0.022		Craddock and Dauphas (2011)	
BHVO-1		Basalt		0.17			0.04		0.11		0.09		This study	
				0.161			0.012		0.105		0.008		Craddock and Dauphas (2011)	

geostandard (BHVO-1), which suggested that the external long-term reproducibility (2σ) for $\delta^{56}Fe$ measurements using this method is ±0.10‰ (Zhao et al., 2012; Sun et al., 2013).

3.2.3. Fe species extraction

The different iron species including Fe-carbonate, Fe-oxide and Fe-magnetite, were extracted following the method established by Poulton and Canfield (2005). 200 mg of sample powder was firstly treated with a buffered sodium acetate solution for 48 h to extract Fe-carbonate phase (Siderite and Ankerite). The residual sample was then extracted with a sodium dithionite solution for 2 h to liberate crystalline ferric oxides (e.g. Ferrihydrite, Goethite and Hematite). Finally, the sample was treated with an ammonium oxalate solution for 6 h to dissolve magnetite. Fe contents were measured by Atomic Absorption Spectrometry (AAS). The Fe-pyrite fraction was calculated from Ag_2S produced by the chromous chloride distillation (Canfield et al., 1986).

3.2.4. Carbon isotope analysis

The carbon isotope analysis was carried out at the Institute of Geochemistry, Chinese Academy of Sciences. About 0.5–5 mg of sample powder was reacted with 10 ml anhydrous H_3PO_4 for 10 min at 90 °C in a Multi-prep inlet system connected to a Finnigan MAT 253 Mass Spectrometer. Isotopic results are expressed in the standard notation as per mil (‰) deviation from V-PDB ($\delta^{13}C_{carb}$). Uncertainties determined by multiple measurements of NBS-19 (TS-limestone) were better than 0.05‰ (1σ).

4. RESULTS

4.1. Major and trace elements

Most cherts from the two sections usually contain lower Fe_2O_3 (<0.78%), Al_2O_3 (<0.33%), Zr (<1.62 ppm) and total rear earth elements (TREE) (<20.20 ppm), but higher SiO_2 (>67.98%) than dolostones and phosphorites (Table 1). Only two cherts (BGY04, 05) from the BGY section show higher Al_2O_3 (0.31–0.53%) and TREE contents (51.57–71.67 ppm). Fe/Al ratios of all samples are close to or higher than that of average crust (0.55, Lyons and Severmann, 2006).

4.2. Fe isotopic composition

All of the cherts investigated in this study yield more positive $\delta^{56}Fe$ values than those of modern oxic deep-sea cherts (−0.48‰ to +0.23‰, Rouxel et al., 2003) (Table

Table 2
The distribution of iron species in samples from the Baiguoyuan (BGY) section and the Liuhuiwan (LHW) section.

Samples	Discription	Depth (m)	Fe_{car} %	Fe_{ox} %	Fe_{mag} %	Fe_{py} %	Fe_{HR} %	Fe_{Sili} %	Fe_T %	Fe_{HR}/Fe_T	Fe_{py}/Fe_{HR}
Liuhuiwan Section											
LHW02	Chert	−3.5	0.003	0.013	0.006	0.006	0.03	0.02	0.05	0.56	0.2
LHW03	Chert	−5.0	0.005	0.006	0.008	0.011	0.03	0.01	0.04	0.75	0.37
LHW04	Chert	−6.0	0.003	0.008	0.011	0.011	0.03	0.01	0.04	0.79	0.34
LHW05	Chert	−6.5	0.003	0.006	0.008	0.006	0.02	0.04	0.06	0.41	0.25
LHW06	Dolostone	−7.0	0.025	0.018	0.016	0.005	0.06	0.23	0.29	0.22	0.08
LHW07	Chert	−8.0	0.005	0.01	0.01	0.004	0.03	0.04	0.07	0.42	0.14
LHW09	Chert	−9.0	0.003	0.008	0.008	0.006	0.02	0.06	0.08	0.29	0.23
LHW10	Chert	−10.5	0.002	0.009	0.005	0.004	0.02	0.03	0.05	0.41	0.19
LHW15	Phosphorite	−13.9	0.001	0.011	0.023	0.002	0.04	0.13	0.17	0.22	0.06
LHW23	Chert	−18.0	0.007	0.017	0.035	0.022	0.08	0.24	0.32	0.26	0.27
LHW23	Chert	−18.0	0.007	0.017	0.035	0.022	0.08	0.24	0.32	0.26	0.27
LHW24	Chert	−19.0	0.009	0.009	0.027	0.006	0.05	0.05	0.1	0.51	0.11
LHW25	Chert	−20.0	0.009	0.008	0.026	0.017	0.06	0.07	0.13	0.47	0.28
LHW26	Chert	−21.0	0.002	0.003	0.002	0.002	0.01	0.01	0.02	0.44	0.2
LHW27	Dolostone	−22.0	0.006	0.03	0.08	0.005	0.12	0.38	0.5	0.24	0.04
Baiguoyuan Section											
BGY03	Chert	−20	0.001	0.006	0.009	0	0.02	0.02	0.04	0.44	0
BGY04	Chert	−20.5	0.003	0.016	0.036	0.011	0.07	0.11	0.18	0.37	0.17
BGY05	Chert	−22.5	0.003	0.011	0.011	0.006	0.03	0.04	0.07	0.43	0.19
BGY06	Dolostone	−23	0.006	0.01	0.013	0.002	0.03	0.17	0.2	0.15	0.07
BGY07	Chert	−27.5	0.003	0.003	0.003	0	0.01	0	0.01	0.71	0
BGY08	Chert	−28.7	0.008	0.015	0.04	0.08	0.14	0.41	0.55	0.26	0.56
BGY10	Chert	−29	0.003	0.007	0.051	0.009	0.07	0.03	0.1	0.72	0.13
BGY11	Dolostone	−30	0.039	0.026	0.09	0.004	0.16	0.25	0.41	0.38	0.03
BGY13	Chert	−33	0.011	0.006	0.004	0.004	0.02	0.02	0.04	0.7	0.17
BGY14	Phosphorite	−94	0.001	0.021	0.026	0.012	0.06	0.26	0.32	0.19	0.2
BGY27	Phosphorite	−96	0	0.033	0.053	0.014	0.1	0.48	0.58	0.17	0.14
BGY29	Phosphorite	−100	0.001	0.03	0.096	0.009	0.14	0.5	0.64	0.21	0.06

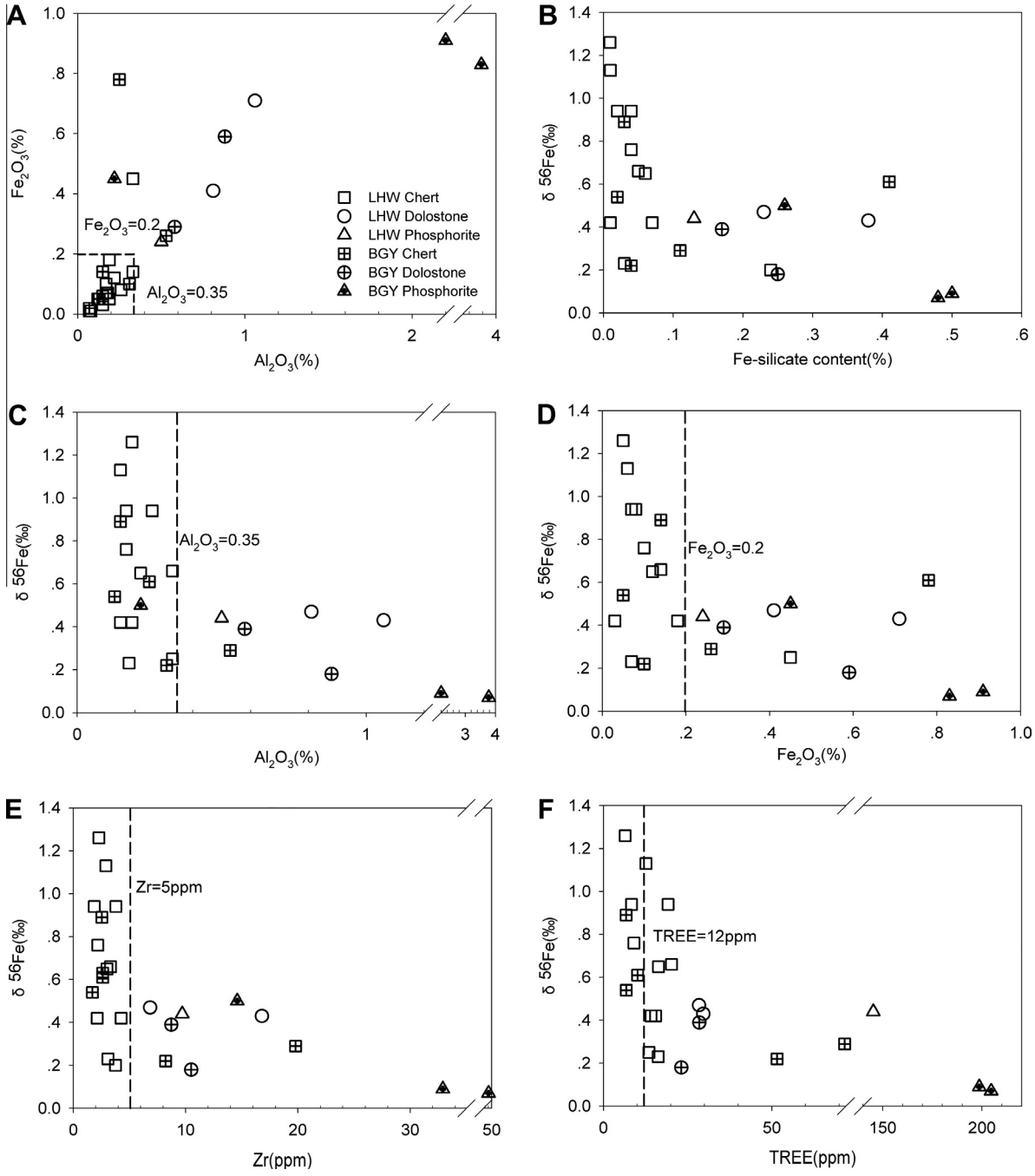

Fig. 3. Crossplots of Fe_2O_3 content against Al_2O_3 content (A), and $\delta^{56}Fe$ value versus Fe-silicate content (B), Al_2O_3 content (C), Fe_2O_3 content (D), Zr content (E) and TREE content (F) show two Fe isotopic end-members including detritus Fe with near zero $\delta^{56}Fe$ value and highly reactive Fe (Fe_{HR}) with positive but variable $\delta^{56}Fe$ value. These dash lines represent a criteria of negligible contamination of detritus, $Al_2O_3 < 0.35\%$, $Fe_2O_3 < 0.20\%$, Zr < 5 ppm and TREE < 12 ppm, following Ling et al. (2013) and based on our data.

1). The $\delta^{56}Fe$ value of the cherts from the LHW section varied in a wide range from 0.20 ± 0.04 to $1.26 \pm 0.10‰$. The cherts from the BGY section also show a broad range of $\delta^{56}Fe$ values ranging from 0.22 ± 0.20 to $0.89 \pm 0.04‰$. The $\delta^{56}Fe$ values of dolostones from two sections cannot be distinguished, with an average of $0.37 \pm 0.13‰$. One of the phosphorites from the BGY section shows the same $\delta^{56}Fe$ value (0.44‰) as those from the LHW section. Another two phosphorites from the BGY section show near zero $\delta^{56}Fe$ values (on average 0.08‰).

4.3. Carbon isotopic composition

A narrow range of $\delta^{13}C_{carb}$ values were obtained, varying from 2.87‰ to −2.03‰ for all samples from the LHW section, whereas those from the BGY section show a

broader range from 5.70‰ to −5.77‰ (Table 1). There are two negative $\delta^{13}C_{carb}$ excursions preserved in upper cherts (BGY05) and lower phosphorites of the BGY section. The upper negative $\delta^{13}C_{carb}$ excursion of the BGY section could easily correspond with the negative $\delta^{13}C_{carb}$ excursion in the LHW section, which is consistent with published data (Zhu et al., 2013).

4.4. Fe speciation

Fe species data (Table 2) indicates that most of the highly reactive Fe (Fe_{HR}) is present as ferric oxides (hematite, goethite and magnetite) rather than ferrous pyrite (generally <15%, except LHW03, 04) and carbonate in cherts, dolostones and phosphorites. In addition to highly reactive Fe, abundant Fe-silicate was observed in dolostones, phosphorites and three cherts (LHW09, 23, BGY08). These samples commonly show lower Fe_{HR}/Fe_T ratios (generally <0.29). The higher Fe_{HR}/Fe_T ratio samples (>0.38) were recorded in most of the cherts from two investigated sections. Most of our samples show very low Fe_{Py}/Fe_T ratios (generally <0.37, except BGY08).

5. DISCUSSION

5.1. Fe isotopic composition

The $\delta^{56}Fe$ values of the whole rock analyses were controlled by the relative amounts of different Fe-bearing minerals, such as ferric oxides (hematite, goethite and magnetite), ferrous pyrite and carbonate, and Fe-silicate from continental detritus. Although Fe isotopic fractionation was dominantly produced by redox reaction of different Fe-minerals, previous studies suggested that early diagenetic processes and later alteration could also result in Fe isotopic fractionation. In this section, effects of different processes on Fe isotopic composition of whole rocks will be discussed in detail.

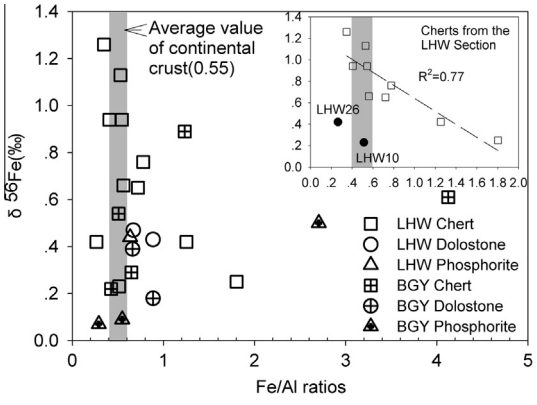

Fig. 4. Relationship between $\delta^{56}Fe$ value and Fe/Al molar ratio. Samples show a broad range of $\delta^{56}Fe$ value at near-continental crust Fe/Al ratio. A negative correlation ($R^2 = 0.77$, except LHW10, 26) has been observed in the LHW section which could reflect weak diagenetic effect. Nonetheless, these observations indicated that early diagenetic alteration had not produced significant Fe isotopic fractionation in our samples.

5.1.1. Detrital effects

Fe speciation data show that abundant detrital Fe-silicate is present in dolostones, phosphorites and some cherts. Silicate minerals commonly contain higher TREE, Al and Zr contents (Nothdurft et al., 2004). Therefore, the positive correlation between Fe and Al (Fig. 3A) indicates the significant influence of Fe-detritus on total Fe content. The correlation between $\delta^{56}Fe$ value and Fe-silicate content, Al_2O_3, Fe_2O_3, Zr and TREE contents for all samples (Fig. 3) indicate that Fe-detritus content could play an important role in diluting $\delta^{56}Fe$ signal of the whole rocks. There are two end-members that can be recognized to explain $\delta^{56}Fe$ values recorded in whole rocks: (1) continental detritus with higher Al, Zr and TREE contents, and near zero $\delta^{56}Fe$ values (0.05‰, Beard et al., 2003); (2) highly reactive $Fe(II)_{aq}$ with positive but varied $\delta^{56}Fe$ dependent on the redox condition. Following a previous study (Ling et al., 2013) and based on our data, a criteria of negligible contamination of detritus (Al < 0.35%, Fe < 0.20%, Zr < 5 ppm and TREE < 12 ppm) was used to estimate $\delta^{56}Fe$ value of our samples. Most of the cherts satisfy the composition criteria and show a broad range of $\delta^{56}Fe$ values, suggesting that $\delta^{56}Fe$ values of the whole rocks were not significantly influenced by Fe-detritus from continental sources, but by other processes.

5.1.2. Early Diagenetic effects

Early diagenetic processes could include dissimilatory iron reduction (DIR) (Severmann et al., 2006) and bacterial sulfate reduction (Xiao et al., 2010) associated with organic matter oxidation. DIR could significantly change the Fe isotopic composition of individual Fe-bearing minerals in sediments and diagenetic pore waters (e.g., Severmann et al., 2006; Staubwasser et al., 2006; Frost et al., 2007), although the process can only represent a minimum of total inventory of Fe cycled by bacteria (Heimann et al., 2010). Partial microbial reduction of iron oxide would produce a negative $\delta^{56}Fe$ value in the released $Fe(II)_{aq}$ and a positive $\delta^{56}Fe$ value in the remaining iron oxide, because of the large isotopic fractionation (−3‰ to −1.3‰) between released $Fe(II)_{aq}$ and the reactive surface layer on the oxide formed during early diagenesis (Beard et al., 2003; Yamaguchi et al., 2005; Johnson and Beard, 2005). The Fe $(II)_{aq}$ released from primary oxides could be oxidized again under oxic conditions and/or transported to a deep water basin under anoxic conditions (Severmann et al., 2008). Most of our samples yield highly positive $\delta^{56}Fe$ values, which may be caused by the partial oxidative precipitation of Fe_{HR} and/or loss of the lighter Fe isotope by significant dissimilatory iron reduction in early diagenesis. The loss of the lighter Fe isotope should be accompanied with decreasing Fe/Al ratios (Severmann et al., 2006, 2008; Asael et al., 2013) if there are significant dissimilatory iron reduction in early diagenesis, which is contrary to our samples proximity to continental sources or higher Fe/Al values. A rough negative correlation between $\delta^{56}Fe$ values and Fe/Al ratios has been observed in cherts from the LHW section ($R^2 = 0.77$, Fig. 4), which could indicate small loss of the lighter Fe isotope by dissimilatory iron reduction from sediments and subsequent transfer of the lighter Fe isotope

from shelf to basin during early diagenesis. Anderson and Raiswell (2004) suggested that about 40% of highly reactive iron initially deposited in modern continental margin sediments can be transformed to dissolved ferrous iron and suspended iron oxides by DIR during early diagenesis, and then transported to deep basin. However, the microbial DIR during diagenesis was significantly decreased by 10 times under alkaline condition with dissolved Si (Wu et al., 2009). Therefore, we proposed that effect of DIR on Fe isotope of whole rocks was significantly discounted.

In addition, the cherts in our study area represent the silicification and replacement of primary carbonate during the early digenetic process (Xiao et al., 2010), although the direct precipitation of authigenic silica from seawater also occurred. Fe isotopic fractionation and chemical cycling during silicification are not well known. Busigny and Dauphas (2007) found that the abiotic dissolution of Fe-oxides did not produce significant Fe isotope fractionation during diagenesis. Regardless, we assumed that silicification grade should be correlated with δ^{56}Fe values and Fe content, if Fe isotopic composition and chemical cycling were directly affected by silicification. However, the absence of correlations between the SiO_2 content and δ^{56}Fe value and Fe/Al ratios suggests that silicification did not produce significant Fe isotopic fractionation during early diagenesis. Therefore, we argue that most of cherts preserved the primary Fe isotopic signature of the whole rocks during deposition, rather than that of diagenetic alteration.

5.1.3. Redox environment effects

Discussion of detrital effects suggested that although the presence of abundant Fe from detritus could produce a significant effect on the δ^{56}Fe values of our whole rocks, detrital Fe participates little in redox cycling. In addition, the lighter Fe isotopes are preferentially incorporated into Fe-carbonate phase at isotopic equilibrium conditions (Yamaguchi et al., 2005; Frost et al., 2007; Von Blanckenburg et al., 2008). Fe-carbonate extracted from shales and dolostones in our study area also show negative and uniform Fe isotopic composition (on average −0.4‰, Yan, 2009). The Fe-carbonate content measured in our samples is low and does not show any relation against δ^{56}Fe values, which indicates that the δ^{56}Fe values of the whole rocks were not controlled by Fe-carbonate. In the discussion of the effect of redox condition on Fe isotopic composition, Fe-carbonate and Fe-silicate phases have been cut out based on a simple mass balance equation ($\delta^{56}Fe_T = f_{Silicate}{}^{*}\delta^{56}Fe_{Silicate} + f_{Carbonate}{}^{*}\delta^{56}Fe_{Carbonate} + f_{Pyrite+Ferric\ oxide}{}^{*}\delta^{56}Fe_{Pyrite+Ferric\ oxide}$). The fractions of different Fe-bearing phase were taken from Table 2. The $\delta^{56}Fe_{Silicate}$ value was given as the value of Bulk Silicate Earth (0.05‰) from Beard et al. (2003), and the $\delta^{56}Fe_{Carbonate}$ value was assumed based on the average δ^{56}Fe value (−0.4‰) of Fe-carbonates from Doushantuo Formation in our study area (Yan, 2009). Although the two assumed number could be arbitrary in natural condition, it is should be homogeneous in our local condition. The recalibrated $\delta^{56}Fe_{calibrate}$ represents mixing of the δ^{56}Fe values of pyrite and ferric oxide, which should be strongly controlled by the match ratio of pyrite and ferric oxide.

Experimental studies suggest that ferric oxides are enriched in heavier Fe isotopes by 0.9‰ to 3.0‰ in abiotic oxidation processes relative to initial $Fe(II)_{aq}$ (Bullen et al., 2001; Johnson et al., 2002; Welch et al., 2003), and by 1.5‰ in anoxic photosynthetic processes (Croal et al., 2004). The Fe isotopic equilibrium fractionation between $Fe(II)_{aq}$ and Fe(III)–Si co-precipitates would be enlarged to −3.51‰∼−3.99‰ depending on different Fe/Si molar ratios (Wu et al., 2012b). By contrast, Fe-sulfides become enriched in the lighter Fe isotopes by −0.3‰ to −0.9‰ in FeS_m phases (Butler et al., 2005) and −3.0‰ to −1.7‰ in pyrite during kinetic fractionation processes (Guilbaud et al., 2011). The Fe isotope fractionation associated with FeS precipitation can be 0.32 ± 0.29‰ relative to initial $Fe(II)_{aq}$ when kinetic isotopic fractionation evolves towards equilibrium (Wu et al., 2012a). Recently, Busigny et al.(2014) suggested that kinetic fractionation of Fe isotope is not significant for pyrite formed under ferruginous

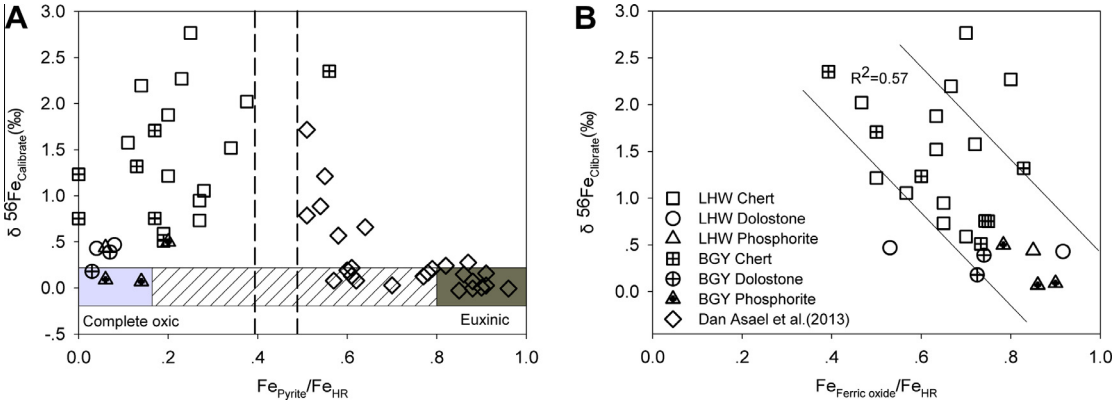

Fig. 5. The recalibrated δ^{56}Fe values of whole rocks plotted against Fe_{Pyrite}/Fe_{HR} and $Fe_{Ferric\ oxide}/Fe_{HR}$ values. (A): Three distinct redox conditions can be recognized: (1) the oxic condition, (2) the anoxic/ferruginous condition, (3) the euxinic condition. The recalibrated δ^{56}Fe could reach a peak value in dash lines zone. (B): The rough negative correlation between δ^{56}Fe values and $Fe_{Ferric\ oxide}/Fe_{HR}$ values indicated that highly positive δ^{56}Fe values reflect lower oxidation degree of $Fe(II)_{aq}$ in seawater column, in turn, lower and near zero δ^{56}Fe values point to higher oxidation degree. R^2 was calculated from samples located between two straight lines.

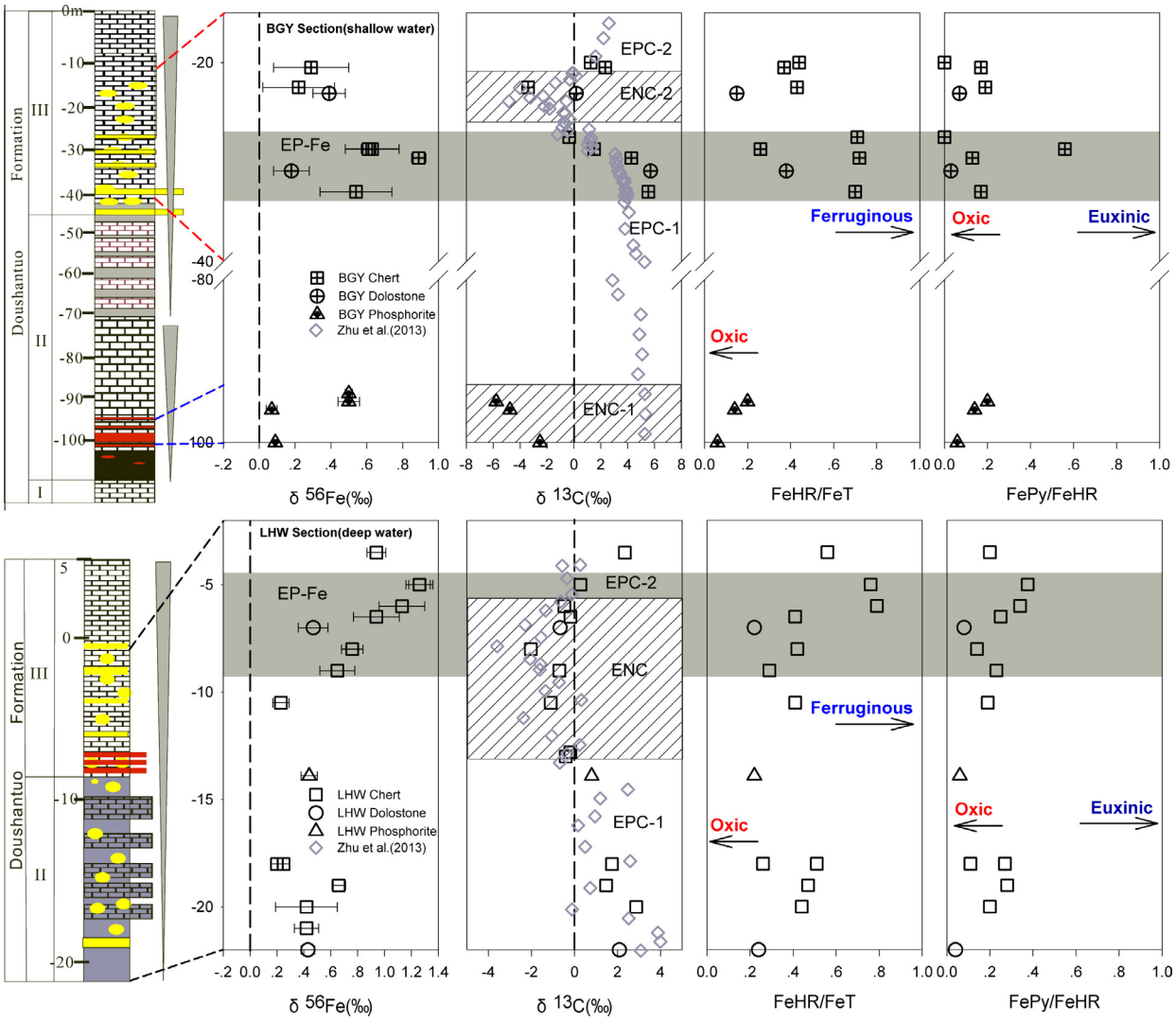

Fig. 6. Comparison of chemostratigraphic profiles of the Doushantuo Formation at the BGY section (shallow water) and the LHW section (deep water), with proposed chemostratigraphic correlation for Fe isotopic composition (grey shading). The major features of the calibrated $\delta^{56}Fe$ (EP-Fe), $\delta^{13}C_{carb}$ value (ENC, ENC1, ENC2, EPC1 and EPC2) and Fe species (relative redox trend) are labeled.

system. The quantitative oxidation and sulfidation of $Fe(II)_{aq}$ in modern oxic/euxinic oceans can minimize the fractionation of Fe isotopes. However, significant Fe isotopic fractionation has been observed during partial oxidation and sulfidation of $Fe(II)_{aq}$ from the Archean ocean with abundant $Fe(II)_{aq}$ (Johnson et al., 2003, 2008; Rouxel et al., 2005). Positive $\delta^{56}Fe$ values for Archean oceanic sedimentary ferric oxide is generally considered to result from partial oxidation of $Fe(II)_{aq}$ in anoxic seawater (Johnson et al., 2008; Heimann et al., 2010; Fabre et al., 2012; Li et al., 2013).

Fig. 5 shows that the $\delta^{56}Fe_{calibrate}$ values of our samples were strongly controlled by different redox conditions: (1) an oxic condition with the $\delta^{56}Fe_{calibrate}$ values near that of seawater, abundant ferric oxide and little pyrite, metrics that reflect quantitative oxidation of $Fe(II)_{aq}$ in a completely oxic seawater column; (2) an anoxic/ferruginous condition (transition between euxinic and oxic) with the positive but varied $\delta^{56}Fe_{calibrate}$ values, intermediate ferric oxide and pyrite content, implying partial oxidation of $Fe(II)_{aq}$ by free O_2 and other oxidants in anoxic seawater; 3) an euxinic condition with the $\delta^{56}Fe$ values near that of seawater, abundant pyrite and little ferric oxide, representing complete sulfidation of $Fe(II)_{aq}$ under H_2S-rich conditions (Rouxel et al., 2005; Duan et al., 2010; Asael et al., 2013). The positive correlation of $\delta^{56}Fe_{calibrate}$ with Fe_{Pyrite}/Fe_{HR} (Fig. 5A) and the rough negative correlation between $\delta^{56}Fe_{calibrate}$ and $Fe_{Ferric\ oxide}/Fe_{HR}$ (Fig. 5B) suggest that the $\delta^{56}Fe_{calibrate}$ values were controlled by the relative proportion of pyrite and ferric oxide. Recently, a dispersion/reaction model (Czaja et al., 2012; Li et al., 2013) was applied to estimate the $Fe(II)_{aq}$ and $Fe(OH)_3$ content and Fe isotopic values along water profiles (200–500 m) based on the oxygen level (0.02–2% of modern O_2) and the rate of $Fe(II)_{aq}$ oxidation (10^{-4} to 10^{-2} mmol L^{-1} day^{-1}). The major conclusion is that quantitative oxidation of $Fe(II)_{aq}$

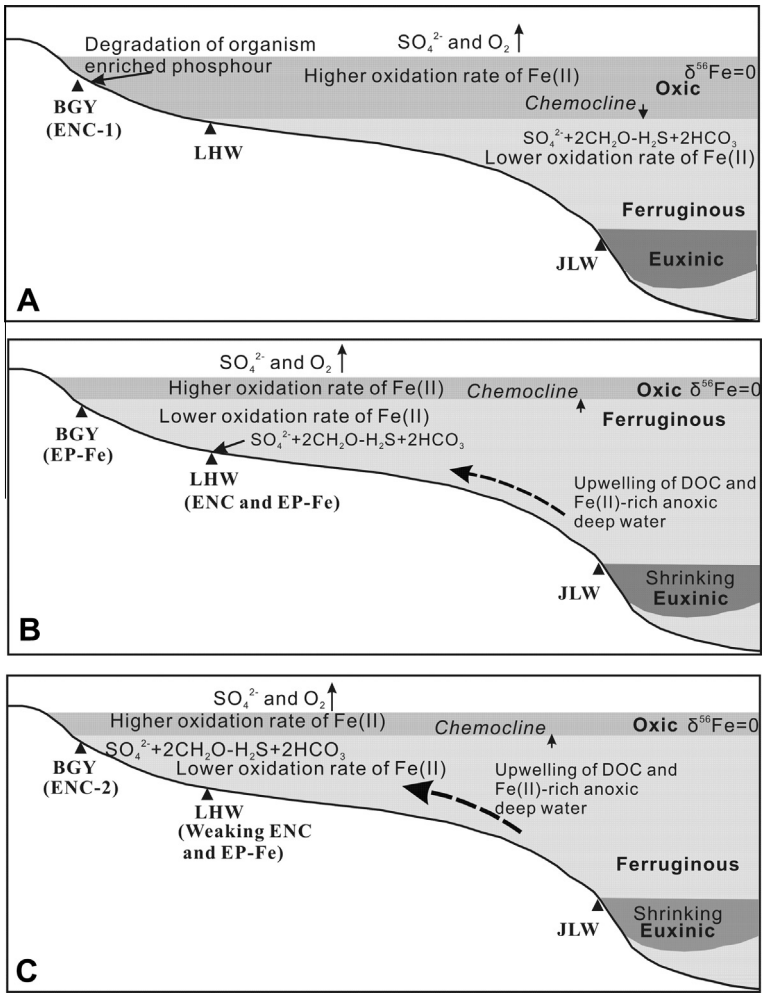

Fig. 7. Schematic diagram illustrating redox chemical change and negative carbon isotopic excursion at the lower Member II and middle Member III in Doushantuo Formation from the Baiguoyuan and Liuhuiwan sections, based on Fe isotopic and speciation and C isotopic data from our study and previous publications. (A): a strongly redox stratified structure is preserved although increasing of sulfate and oxygen had lowered the chemocline depth. During the interval, higher oxidation rate of $Fe(II)_{aq}$ occurred under oxic shallow water, and lower rate was presented under ferruginous deep water. A negative $\delta^{13}C_{carb}$ excursion (ENC-1) recorded in phosphorites from the Baiguoyuan section could result from oxidation of organism containing phosphorus. (B): During times of increased supply of $Fe(II)_{aq}$ and dissolved organic carbon (DOC) from upwelling anoxic deep water, chemocline fluctuations and oxidation of DOC in oxic shallow seawater resulted in a negative $\delta^{13}C_{carb}$ excursion (ENC) at the Liuhuiwan section, and lower oxidation rate of $Fe(II)_{aq}$ leads to positive Fe isotopic shift (EP-Fe) at the two studied sections. (C): Continuously increased upwelling of $Fe(II)_{aq}$ and DOC-rich anoxic deep water leads to a lagging negative $\delta^{13}C_{carb}$ excursion (ENC-2) at shallower Baiguoyuan section and weaking negative $\delta^{13}C_{carb}$ excursion and positive $\delta^{56}Fe$ excursion at deeper Liuhuiwan section. Meanwhile, exhaustion of sulfate by oxidation of upwelling $Fe(II)_{aq}$ and DOC-rich anoxic deep water in oxic shallow water results in less sulfate penetration downward to deep water, which would shrink euxinic zone at Jiulongwan section (B and C).

by both high oxygenic conditions and/or high activity of anoxygenic photosynthesis would result in near zero $\delta^{56}Fe$ values recorded in precipitated $Fe(OH)_3$. In contrast, partial oxidation of $Fe(II)_{aq}$ would produce $Fe(OH)_3$ with a highly positive $\delta^{56}Fe$ value (Czaja et al., 2012; Li et al., 2013). Therefore, the positive $\delta^{56}Fe_{calibrate}$ values, high pyrite content and low Fe-oxide content in most of cherts from the two studied sections reflects limited oxidation of $Fe(II)_{aq}$ in an anoxic, Fe(II)-rich water body. Highly positive $\delta^{56}Fe$ values of Achaean Marble Bar Chert were also reported by Li et al. (2013) who proposed that extreme positive $\delta^{56}Fe$ values (1.5–2.6‰) require a low level of oxidation under $Fe(II)_{aq}$-rich seawater. Conversely, low $\delta^{56}Fe_{calibrate}$ values, low pyrite content and abundant Fe-oxides in all of our phosphorites and dolostones should be consistent with completely oxic conditions.

When the pyrite content was dominant in samples, the same range of $\delta^{56}Fe_{calibrate}$ values occurred on the right side of the two dash lines. However, this zone reflects more oxygen-depleted conditions or even euxinic conditions (Fig. 5A), which can be confirmed by recent studies (Duan et al., 2010; Asael et al., 2013). The rough negative correlation between $\delta^{56}Fe_{calibrate}$ and Fe_{Py}/Fe_{HR} values indicates that $\delta^{56}Fe_{calibrate}$ was controlled by the increase of syn-sedimentary pyrite in more O_2-depleted water. Under H_2S-rich conditions, the $Fe(II)_{aq}$ in seawater

becomes rapidly fixed as FeS_m, and then precipitated as pyrite that inherits the Fe isotopic composition of the ambient seawater (Rouxel et al., 2005; Nishizawa et al., 2010).

5.2. Constrains for oxygenation of Edicaran Ocean

A recent study has suggested that the Ediacaran Ocean was characterized by a redox chemical stratification model, with oxic surface water underlain by a thin ferruginous layer, an euxinic wedge and ferruginous deep water based on Fe species data (Li et al., 2010). Fe isotopic and speciation data (Fig. 6) suggest that phosphorite deposits interlaminated with dolostones at the lower part of the BGY section were formed under completely oxic conditions (Fig. 7A). These phosphorites deposited on the shallow shelf may have been associated with high productivity areas fertilized by weathering inputs. High sulfate availability could then promote phosphogenesis through organic matter degradation and enrichment of phosphorite through Fe-redox pumping (Jiang et al., 2011). Higher detrital Fe and ferric oxide contents, near zero $\delta^{56}Fe$ values, and negative $\delta^{13}C_{carb}$ excursions preserved in phosphorite also provide potent evidence for the model. Dolostones from the lower part of the LHW section also recorded an oxic condition.

However, cherts from the basal LHW section reflect a ferruginous condition (Fig. 6), consistent with widespread ferruginous water in a shallow continental basin, outer shelf and deep basin, as proposed by Canfield et al. (2008). The redox fluctuation between oxic and ferruginous conditions and strongly variable Fe/Al ratios at the basal LHW section indicate that the LHW section was located near the boundary of an oxic and anoxic layer (Fig. 7A). Episodic euxinic conditions have been recorded at the lower part of Member II of the Jiulongwan (JLW) section (Li et al., 2010). Therefore, the redox chemical stratification model with oxic and ferruginous shallow shelf water suggests that oxic conditions did not dominate the Early Ediacaran Ocean (Fig. 7A).

It is important to note that the positive $\delta^{56}Fe$ and negative $\delta^{13}C_{carb}$ excursions were observed in the uppermost portion of the two studied sections (Fig. 6). These negative $\delta^{13}C_{carb}$ excursions have been previously observed in many sections from the Yangtze Gorges area (Jiang et al., 2007; Zhu et al., 2013) that correspond with the second negative $\delta^{13}C_{carb}$ excursion (ENC2) in the JLW section (Jiang et al., 2007; McFadden et al., 2008; Li et al., 2010). It is generally considered that the ENC2 resulted from a large pulse of oxidation of the oceanic DOC pool by sulfate reduction in at least mildly oxygenated deep ocean waters, rather than the mixing of detrital organic carbon or alteration and diagenesis (Fike et al., 2006; Jiang et al., 2007, 2011; McFadden et al., 2008; Bjerrum and Canfield, 2011). The model of DOC oxidation by increasing sulfate and oxygen would lower chemocline of Ediacaran Ocean (Jiang et al., 2007, 2011).

However, Fe isotopic and other geochemical data (Fig. 6) in the upper parts of two studied sections reflect a return to more reducing conditions than that of the lower part of Member II (Fig. 7B and C). This phenomenon is consistent with transgressive systems (Li et al., 2010; Zhu et al., 2013). An interpretation for the positive $\delta^{56}Fe$ excursion occurred at these places is that the upwelling of anoxic $Fe(II)_{aq}$- and DOC-rich deep water lower the oxidation degree of dissolved $Fe(II)_{aq}$ in shallow water. Meanwhile, a part of the dissolved $Fe(II)_{aq}$ can also be removed from seawater by H_2S, which is product of the upwelling anoxic deep water reacting with sulfates in oxic shallow environment (Fig. 7B and C). These two simultaneous processes are responsible for the increase of Fe_{HR}/Fe_T and Fe_{Py}/Fe_T ratios of our samples in this interval. The DOC in upwelling anoxic deep water was also oxidized in the oxic or suboxic shallow water and can explain the negative $\delta^{13}C_{carb}$ excursion (Fig. 7B and C). However, it is noted that the negative $\delta^{13}C_{carb}$ excursion occurred prior to the positive $\delta^{56}Fe$ excursion in the LHW section but after the $\delta^{56}Fe$ excursion in the BGY section (Fig. 6). It suggests that most of the DOC in the upwelling anoxic deep water was oxidized at the LHW location before reaching to the BGY section (Fig. 7B). Only if free oxygen or other oxidants at the LHW place were not enough to oxidized all of DOC in the upwelling anoxic deep water, some of DOC could arrive the BGY section and be oxidized there. In this way, the lagging negative $\delta^{13}C_{carb}$ excursion in the BGY section (Fig. 7C) and the prolonged negative $\delta^{13}C_{carb}$ excursion and the continuous increase of Fe_{HR}/Fe_T and Fe_{Py}/Fe_T ratios in the upper part of the LHW section (Fig. 6) can be well-explained.

The redox status change is also recorded in the JLW section, with a character of fluctuations between euxinic and ferruginous conditions (Fig. 7, Li et al., 2010). The highly positive $\delta^{34}S_{pyrite}$ value (McFadden et al., 2008; Li et al., 2010) can be ascribed to a decrease of sulfate penetration downward into deep water due to the exhaustion of sulfate by oxidation of upwelling DOC-rich anoxic deep water into shallow oxic water body. The oxidation of $Fe(II)_{aq}$ and DOC in upwelling anoxic deep water could result in the shrinking of the euxinic zone and decrease of the DOC pool in the deep water, as well as $Fe(II)_{aq}$ concentrations in the whole ocean, which could result in redox change of Ediacaran ocean.

6. CONCLUSION

This study shows that cherts produced by early diagenesis preserved primitive $\delta^{56}Fe$ signatures of its depositional process, rather than the signature of diagenetic alteration. However for some of our samples characterized by high Al contents, continental detritus could dilute the Fe isotopic signal. Highly positive $\delta^{56}Fe$ values reflect lower rates of oxidation of $Fe(II)_{aq}$ in ferruginous seawater. In contrast, low and near zero $\delta^{56}Fe$ values indicate oxic condition. Together with published geochemical data, our data indicate that oxic conditions had not dominated the Early Ediacaran Ocean, consistent with a redox chemical stratification model proposed by Li et al. (2010).

More importantly, we provide strong evidence for the oxidation mechanism of dissolved organic carbon. Our results do not support the previous hypothesis that the well-known large negative $\delta^{13}C_{carb}$ excursion (ENC2) widespread in the middle of Doushantuo Formation in South China was caused by the continuous oxygenation of seawa-

ter. It should be resulted from the oxidation of DOC upwelling from anoxic deep water into oxic shallow seawater. The oxidation of upwelling Fe $(II)_{aq}$ and DOC-rich anoxic deep water under oxic shallow seawater could result in the shrinking of the euxinic zone and DOC pool in the deep water and the decrease of $Fe(II)_{aq}$ concentrations in the whole ocean, associated with consumption of dissolved oxygen and other oxidants. At the same time, the upwelling of DOC- and Fe(II)-rich anoxic deep water could also produce strong photosynthesis. The balance between oxygen consumption and production would directly promote the further oxygenation of Ediacaran ocean and the evolution of eukaryotic organisms.

ACKNOWLEDGMENT

This project was supported by MLR Public Benefit Research Foundation (201011027, 201411044), the National Natural Science Foundation of China (41273024, 41072145, 41303003), and China Geological Survey Foundation (1212011121069, 1212011120354). We give thanks to Pengju Liu and Maoyan Zhu for helping in field work, Jianxiong Ma, Shizhen Li, Zhihong Li, Feifei Zhang and Aiguo Dong for helping in lab works, Kyle Trostle and Yuzhuo Qiu for improving the manuscript, Vincent Busigny and two anonymous reviewers for reviewing the manuscript.

REFERENCES

Anderson T. F. and Raiswell R. (2004) Sources and mechanisms for the enrichment of highly reactive iron in euxinic Black Sea sediments. *Am. J. Sci.* **304**, 203–233.

Asael D., Tissot F. L. H., Reinhard C. T., Rouxel O., Dauphas N., Lyons T. W., Ponzevera E., Liorzou C. and Cheron S. (2013) Coupled molybdenum, iron and uranium stable isotopes as oceanic paleoredox proxies during the Paleoproterozoic Shunga Event. *Chem. Geol.* **2013**. http://dx.doi.org/10.1016/j.chemgeo.08.003.

Beard B. L., Johnson C. M., Skulan J. L., Nealson K. H., Cox L. and Sun H. (2003) Application of Fe isotopes to tracing the geochemical and biological cycling of Fe. *Chem. Geol.* **195**, 87–117.

Bjerrum C. J. and Canfield D. E. (2011) Towards a quantitative understanding of the late Neoproterozoic carbon cycle. *Proc. Natl. Acad. Sci.* **108**, 5542–5547.

Bullen T. D., White A. F., Childs C. W., Vivit D. V. and Schulz M. S. (2001) Demonstration of significant abiotic iron isotope fractionation in nature. *Geology* **29**, 699–702.

Busigny V. and Dauphas N. (2007) Tracing paleofluid circulations using iron isotopes: a study of hematite and goethite concretions from the Navajo Sandstone (Utah, USA). *Earth Planet. Sci. Lett.* **254**, 272–287.

Busigny V., Planavsky N. J., Jézéquel D., Crowe S., Louvat P., Moureau J., Viollier E. and Lyons T. W. (2014) Iron isotopes in an Archean ocean analogue. *Geochim. Cosmochim. Acta* **133**, 443–462.

Butler I. B., Archer C., Vance D., Oldroyd A. and Rickard D. (2005) Fe isotope fractionation on FeS formation in ambient aqueous solution. *Earth Planet. Sci. Lett.* **236**, 430–442.

Canfield D. E. (2005) The early history of atmospheric oxygen: homage to Robert M. Garrels. *Annu. Rev. Earth Planet. Sci.* **33**, 1–36.

Canfield D. E., Poulton S. W. and Narbonne G. M. (2007) Late-Neoproterozoic deep-ocean oxygenation and the rise of animal life. *Science* **315**, 92–95.

Canfield D. E., Poulton S. W., Knoll A. H., Narbonne G. M., Ross G., Goldberg T. and Strauss H. (2008) Ferruginous conditions dominated later Neoproterozoic deep water chemistry. *Science* **321**, 949–952.

Canfield D. E., Raiswell R., Westrich J. T., Reaves C. M. and Berner R. A. (1986) The use of chromium reduction in the analysis of reduced inorganic sulfur in sediments and shales. *Chem. Geol.* **54**, 149–155.

Condon D., Zhu M., Bowring S., Wang W., Yang A. and Jin Y. (2005) U–Pb ages from the Neoproterozoic Doushantuo formation, China. *Science* **308**, 95–98.

Craddock P. R. and Dauphas N. (2011) Iron isotopic compositions of geological refer-ence materials and chondrites. *Geostand. Geoanal. Res.* **35**, 101–123.

Croal L. R., Johnson C. M., Beard B. L. and Newman D. K. (2004) Iron isotope fractionation by Fe(II)-oxidizing photoautotrophic bacteria. *Geochim. Cosmochim. Acta* **68**, 1227–1242.

Czaja A. D., Johnson C. M., Roden E. E., Beard B. L., Voegelin A. R., Nagler T. F., Beukes N. J. and Wille M. (2012) Evidence for free oxygen in the Neoarchean ocean based on coupled iron-molybdenum isotope fractionation. *Geochim. Cosmochim. Acta* **86**, 118–137.

Derry L. A. (2010) A burial diagenesis origin for the Ediacaran Shuram-Wonoka carbon isotope anomaly. *Earth Planet. Sci. Lett.* **294**, 152–162.

Duan Y., Severmann S., Anbar A. D., Lyons T. W., Gordon G. W. and Sageman B. B. (2010) Isotopic evidence for Fe cycling and repartitioning in ancient oxygen-deficient settings: examples from black shales of the mid-to-late Devonian Appalachian basin. *Earth Planet. Sci. Lett.* **290**, 244–253.

Fabre S., Nédélec A., Poitrasson F., Strauss H., Thomazo C. and Nogueira A. (2011) Iron and sulphur isotopes from the Carajás mining province (Pará, Brazil): implications for the oxidation of the ocean and the atmosphere across the Archaean-Proterozoic transition. *Chem. Geol.* **289**, 124–139.

Fike D. A., Grotzinger J. P., Pratt L. M. and Summons R. E. (2006) Oxidation of the Ediacaran Ocean. *Nature* **444**, 744–747.

Frost C. D., von Blanckenburg F., Schoenberg R., Frost B. R. and Swapp S. M. (2007) Preservation of Fe isotope heterogeneities during diagenesis and metamorphism of banded iron-formation. *Contrib. Mineral. Petrol.* **153**, 211–235.

Guilbaud R., Butler I. B. and Ellam R. M. (2011) Abiotic pyrite formation produces a large Fe isotope fractionation. *Science* **332**, 1548–1551.

Heimann A., Johnson C. M., Beard B. L., Valley J. W., Roden E. E., Spicuzza M. J. and Beukes N. J. (2010) Fe, C, and O isotope compositions of banded iron formation carbonates demonstrate a major role for dissimilatory iron reduction in 2.5 Ga marine environments. *Earth Planet. Sci. Lett.* **294**, 8–18.

Jiang G., Kaufman A. J., Christie-Blick N., Zhang S. and Wu H. (2007) Carbon isotope variability across the Ediacaran Yangtze platform in South China: implications for a large surface-to-deep ocean $\delta^{13}C$ gradient. *Earth Planet. Sci. Lett.* **261**, 303–320.

Jiang G., Shi X., Zhang S., Wang Y. and Xiao S. (2011) Stratigraphy and paleogeography of the Ediacaran Doushantuo Formation (ca. 635–551 Ma) in South China. *Gondwana Res.* **19**, 831–849.

Jiang G., Sohl L. E. and Christie-Blick N. (2003) Neoproterozoic stratigraphic comparison of the Lesser Himalaya (India) and Yangtze block (south China): paleogeographic implications. *Geology* **31**, 917–920.

Johnson C. M., Beard B. L., Beukes N. J., Klein C. and O'Leary J. M. (2003) Ancient geochemical cycling in the Earth as inferred from Fe isotope studies of banded iron formations from the Transvaal Craton. *Contrib. Mineral. Petrol.* **144**, 523–547.

Johnson C. M. and Beard B. L. (2005) Biogeochemical cycling of iron isotopes. *Science* **309**, 1025–1027.

Johnson C. M., Beard B. L., Klein C., Beukes N. J. and Roden E. E. (2008) Iron isotopes constrain biologic and abiologic processes in banded Iron formation genesis. *Geochim. Cosmochim. Acta* **72**, 151–169.

Johnson C. M., Roden E. E., Welch S. A. and Beard B. L. (2005) Experimental constraints on Fe isotope fractionation during magnetite and Fe carbonate formation coupled to dissimilatory hydrous ferric oxide reduction. *Geochim. Cosmochim. Acta* **69**, 963–993.

Johnson C. M., Skulan J. L., Beard B. L., Sun H., Nealson K. H. and Braterman P. S. (2002) Isotopic fractionation between Fe(III) and Fe(II) in aqueous solutions. *Earth Planet. Sci. Lett.* **195**, 141–153.

Knauth L. P. and Kennedy M. J. (2009) The late Precambrian greening of the Earth. *Nature* **460**, 728–732.

Li C., Love G. D., Lyons T. W., Fike D. A., Sessions A. L. and Chu X. (2010) A stratified redox model for the Ediacaran Ocean. *Science* **328**, 80–83.

Li W., Czaja A. D., Van Kranendonk M. J., Beard B. L., Roden E. E. and Johnson C. M. (2013) An anoxic, Fe(II)-rich, U-poor ocean 3.46 billion years ago. *Geochim. Cosmochim. Acta* **120**, 65–79.

Ling H., Chen X., Li D., Wang D., Shields-Zhou G. A. and Zhu M. (2013) Cerium anomaly variations in Ediacaran-earliest Cambrian carbonates from the Yangtze Gorges area, South China: implications for oxygenation of coeval shallow seawater. *Precambr. Res.* **225**, 110–127.

Liu P., Yin C., Chen S., Tang F. and Gao L. (2013) The biostratigraphic succession of acanthomorphic acritarchs of the Ediacaran Doushan-tuo Formation in the Yangtze Gorges area, South China and its biostratigraphic correlation with Australia. *Precambr. Res.* **225**, 29–43.

Lyons T. W. and Severmann S. (2006) A critical look at iron paleoredox proxies: new insights from modern euxinic marine basins. *Geochim. Cosmochim. Acta* **70**, 5698–5722.

McFadden K. A., Huang J., Chu X., Jiang G., Kaufman A. J., Zhou C., Yuan X. and Xiao S. (2008) Pulsed oxygenation and biological evolution in the Ediacaran Doushantuo Formation. *Proc. Natl. Acad. Sci.* **105**, 3197–3202.

McFadden K. A., Xiao S., Zhou C. and Kowalewski M. (2009) Quantitative evaluation of the biostratigraphic distribution of acanthomorphic acritarchs in the Ediacaran Doushantuo Formation in the Yangtze Gorges area, South China. *Precambr. Res.* **173**, 170–190.

Nishizawa M., Yamamoto H., Ueno Y., Tsuruoka S., Shibuya T., Sawaki Y., Yamamoto S., Kon Y., Kitajima K., Komiya T., Maruyama S. and Hirata T. (2010) Grain-scale iron isotopic distribution of pyrite from Precambrian shallow marine carbonate revealed by a femtosecond laser ablation multicollector ICP-MS technique: possible proxy for the redox state of ancient seawater. *Geochim. Cosmochim. Acta* **74**, 2760–2778.

Nothdurft L. D., Webb G. E. and Kamber B. S. (2004) Rare earth element geochemistry of Late Devonian reefal carbonates, Canning Basin Western Australia: confirmation of a seawater REE proxy in ancient limestones. *Geochim. Cosmochim. Acta* **68**, 263–283.

Poulton S. W. and Canfield D. E. (2005) Development of a sequential extraction procedure for iron: implications for iron partitioning in continentally derived particulates. *Chem. Geol.* **214**, 209–221.

Qi L., Hu J. and Gregoire D. C. (2000) Determination of trace elements in granites by inductively coupled plasma mass spectrometry. *Talanta* **51**, 507–513.

Rouxel O. J., Dobbek N., Ludden J. and Fouquet Y. (2003) Iron isotope fractionation during oceanic crust alteration. *Chem. Geol.* **202**, 155–182.

Rouxel O. J., Bekker A. and Edwards K. J. (2005) Iron isotope constraints on the Archean and Paleoproterozoic Ocean redox state. *Science* **307**, 1088–1091.

Sahoo S. K., Planavsky N. J., Kendall B., Wang X., Shi X., Scott C., Scott C., Anbar A. D., Lyons T. W. and Jiang G. (2012) Ocean oxygenation in the wake of the Marinoan glaciation. *Nature* **489**, 546–549, Date published:Pages.

Severmann S., Johnson C. M., Beard B. L. and McManus J. (2006) The effect of early diagenesis on the Fe isotope compositions of porewaters and authigenic minerals in continental margin sediments. *Geochim. Cosmochim. Acta* **70**, 2006–2022.

Severmann S., Lyons T. W., Anbar A. D., McManus J. and Gordon G. (2008) Modern iron isotope perspective on the benthic iron shuttle and the redox evolution of ancient oceans. *Geology* **36**, 487–490.

Shields-Zhou G. and Och L. (2011) The case for a Neoproterozoic oxygenation event: geochemical evidence and biological consequences. *GSA Today* **21**, 4–11.

Staubwasser M., von Blanckenburg F. and Schoenberg R. (2006) Iron isotopes in the early marine diagenetic iron cycle. *Geology* **34**, 629–632.

Sun J., Zhu X., Chen Y. and Fang N. (2013) Iron isotopic constraints on the genesis of Bayan Obo ore deposit, Inner Mongolia. *China. Precambr. Res.* **235**, 88–106.

Von Blanckenburg F., Mamberti M., Schoenberg R., Kamber B. S. and Webb G. E. (2008) The Iron isotope composition of microbial carbonate. *Chem. Geol.* **249**, 113–128.

Wang J. and Li Z. (2003) History of Neoproterozoic rift basins in South China: implications for Rodinia break-up. *Precambr. Res.* **122**, 141–158.

Welch S. A., Beard B. L., Johnson C. M. and Braterman P. S. (2003) Kinetic and equilibrium Fe isotope fractionation between aqueous Fe(II) and Fe(III). *Geochim. Cosmochim. Acta* **67**, 4231–4250.

Wiesli R. A., Beard B. L. and Johnson C. M. (2004) Experimental determination of Fe isotope fractionation between aqueous Fe(II), siderite and "green rust" in abiotic systems. *Chem. Geol.* **211**, 343–362.

Wu L., Beard B. L., Roden E. E. and Johnson C. M. (2009) Influence of pH and dissolved Si on Fe isotope fractionation during dissimilatory microbial reduction of hematite. *Geochim. Cosmochim. Acta* **73**, 5584–5599.

Wu L., Druschel G., Findlay A., Beard B. L. and Johnson C. M. (2012a) Experimental determination of iron isotope fractionations among Fe^{2+}_{aq} –FeS_{aq}–Mackinawite at low temperatures: implications for the rock record. *Geochim. Cosmochim. Acta* **89**, 46–61.

Wu L., Percak-Dennett E. M., Beard B. L., Roden E. E. and Johnson C. M. (2012b) Stable iron isotope fractionation between aqueous Fe(II) and model Archean ocean Fe–Si coprecipitates and implications for iron isotope variations in the ancient rock record. *Geochim. Cosmochim. Acta* **84**, 14–28.

Xiao S. (2004) New multicellular algal fossils and acritarchs in Doushantuo chert nodules (Neoproterozoic, Yangtze Gorges, South China). *J. Paleontol.* **78**, 393–401.

Xiao S., Schiffbauer J. D., McFadden K. A. and Hunter J. (2010) Petrographic and SIMS pyrite sulfur isotope analyses of Ediacaran chert nodules: implications for microbial processes in pyrite rim formation, silicification, and exceptional fossil preservation. *Earth Planet. Sci. Lett.* **297**, 481–495.

Yamaguchi K. E., Johnson C. M., Beard B. L. and Ohmoto H. (2005) Biogeochemical cycling of iron in the Archean-Paleoproterozoic Earth: constraints from iron isotope variations in

sedimentary rocks from the Kaapvaal and Pilbara Cratons. *Chem. Geol.* **218**, 135–169.

Yan B. (2009). Fe isotope features of Cap Carbonates and Black Shales in Doushantuo Formation: ImPlications for Paleo-oeeanography. A dissertation submitted to Chinese Aeademy of Geological Sciences for a master degree. Beijing (In Chinese with English abstract).

Yoshiya K., Nishizawa M., Sawaki Y., Ueno Y., Komiya T., Yamada K., Yoshida N., Hirata T., Wada H. and Maruyama S. (2012) *In situ* iron isotope analyses of pyrite and organic carbon isotope ratios in the Fortescue Group: metabolic variations of a Late Archean ecosystem. *Precambr. Res.* **212–213**, 169–193.

Zhao X., Zhang H., Zhu X., Tang S. and Yan B. (2012) Iron isotope evidence formultistage melt–peridotite interactions in the lithospheric mantle of eastern China. *Chem. Geol.* **292–293**, 127–139.

Zhu M., Lu M., Zhang J., Zhao F., Li G., Yang A., Zhao X. and Zhao M. (2013) Carbon isotope chemostratigraphy and sedimentary facies evolution of the Ediacaran Doushantuo Formation in western Hubei, South China: *Precambr. Res.* **225**, 7–28.

Zhu M., Zhang J. and Yang A. H. (2007) Integrated Ediacaran (Sinian) chronostratigraphy of South China. *Palaeogeogr. Palaeoclimatol. Palaeoecol.* **254**, 7–61.

Zhu X., Li Z., Tang S. and Li Y. (2008a) Fe isotope characteristics of early Precambrian pyrite deposits and their geological signif icance : examples from Shandong and Hebei Provinces. *Acta Petrol. Mineral.* **27**, 429–434 (In Chinese with English abstract).

Zhu X., Li Z., Zhao X., Tang S., He X. and Nick S. (2008b) High-precision measurements of Fe isotopes using MC-ICP-MS and Fe isotope compositions of geological reference materials. *Acta Petrol. Mineral.* **27**, 263–272 (In Chinese with English abstract).

Associate editor: Nicolas Dauphas